

Cosmic ray streaming in the turbulent interstellar medium

SIYAO XU¹ AND ALEX LAZARIAN^{2,3}

¹*Institute for Advanced Study, 1 Einstein Drive, Princeton, NJ 08540, USA; sxu@ias.edu*^a

²*Department of Astronomy, University of Wisconsin, 475 North Charter Street, Madison, WI 53706, USA; lazarian@astro.wisc.edu*

³*Centro de Investigación en Astronomía, Universidad Bernardo O'Higgins, Santiago, General Gana 1760, 8370993, Chile*

ABSTRACT

We study the streaming instability of GeV–100 GeV cosmic rays (CRs) and its damping in the turbulent interstellar medium (ISM). We find that the damping of streaming instability is dominated by ion-neutral collisional damping in weakly ionized molecular clouds, turbulent damping in the highly ionized warm medium, and nonlinear Landau damping in the Galactic halo. Only in the Galactic halo, is the streaming speed of CRs close to the Alfvén speed. Alfvénic turbulence plays an important role in both suppressing the streaming instability and regulating the diffusion of streaming CRs via magnetic field line tangling, with the effective mean free path of streaming CRs in the observer frame determined by the Alfvénic scale in super-Alfvénic turbulence. The resulting diffusion coefficient is sensitive to Alfvén Mach number, which has a large range of values in the multi-phase ISM. Super-Alfvénic turbulence contributes to additional confinement of streaming CRs, irrespective of the dominant damping mechanism.

1. INTRODUCTION

The resonant streaming instability (Wentzel 1974; Kulsrud & Pearce 1969; Wentzel 1969; Skilling 1971) is important for confining cosmic rays (CRs) with energies up to ~ 100 GeV in the Galaxy (Farmer & Goldreich 2004). It has many astrophysical implications on, e.g., shock acceleration (Bell 1978), heating of intracluster media (Guo & Oh 2008; Brunetti & Jones 2014), launching galactic winds (Ipavich 1975; Wiener et al. 2017; Mao & Ostriker 2018; Holguin et al. 2019; Quataert et al. 2021), transport of CRs in starburst galaxies (Krumholz et al. 2020) and around CR sources (Marcowith et al. 2021), and explaining PAMELA and AMS-02 observations at Earth (Blasi et al. 2012; Amato & Casanova 2021).

The self-generated Alfvén waves by CRs via the streaming instability are subject to various damping effects, including ion-neutral collisional damping in a partially ionized medium (Kulsrud & Pearce 1969; Plotnikov et al. 2021; Armillotta et al. 2021), nonlinear Landau damping in a collisionless medium (Kulsrud 2005), as well as turbulent damping by background Alfvénic turbulence (Lazarian 2016). Unlike other damping mechanisms depending on plasma conditions, turbulent damping depends on properties of magnetohydrodynamic (MHD) turbulence. Measurements in different interstellar phases reveal a large range of turbulence parameters, e.g., Alfvén Mach number M_A that characterizes the magnetization level of turbulence (Lazarian et al. 2018; Hu et al. 2019).

Based on the theoretical understanding of MHD turbulence developed since Goldreich & Sridhar (1995) and Lazarian & Vishniac (1999), Farmer & Goldreich (2004) first formulated

the turbulent damping rate for trans-Alfvénic ($M_A = 1$) turbulence. Lazarian (2016) further provided a detailed analysis on turbulent damping in both super-Alfvénic ($M_A > 1$) and sub-Alfvénic ($M_A < 1$) turbulence. When the growth of streaming instability is limited by turbulent damping, the resulting streaming speed of CRs can deviate from the Alfvén speed and is sensitive to turbulence parameters. In addition, due to the magnetic field line tangling in super-Alfvénic turbulence, CRs streaming along turbulent magnetic fields have an effective mean free path determined by the Alfvénic scale $l_A = LM_A^{-3}$ (Lazarian 2006; Brunetti & Lazarian 2007), where L is the injection scale of turbulence, and an isotropic distribution on scales larger than l_A . The above effect on the spatial diffusion of streaming CRs has not been addressed in previous studies.

In this work, we focus on the effect of Alfvénic turbulence on the streaming speed and diffusive propagation of streaming CRs in the energy range GeV–100 GeV in different turbulence regimes. We also examine the relative importance between turbulent damping and other damping mechanisms of streaming instability in various interstellar phases. In particular, in a partially ionized medium, as MHD turbulence is also subject to ion-neutral collisional damping (Xu et al. 2015, 2016; Xu & Lazarian 2017a), the relative importance between turbulent damping and ion-neutral collisional damping of CR-driven Alfvén waves depends on the ionization fraction and the coupling state between ions and neutrals in different ranges of length scales.

The paper is organized as follows. The description on streaming instability and different damping effects is presented in Section 2. In Section 3, we compare turbulent damping and ion-neutral collisional damping in both weakly and highly ionized media, and we derive the corresponding streaming speed and diffusion coefficient in different regimes. The comparison between turbulent damping and

^a Hubble Fellow

nonlinear Landau damping in the Galactic halo is carried out in Section 4. Discussion and our summary are in Section 5 and Section 6, respectively.

2. GROWTH AND DAMPING OF CR-DRIVEN ALFVÉN WAVES

2.1. Growth of Alfvén waves

The same resonance condition, $\lambda \sim r_L$, applies to both gyroresonant scattering of CRs by Alfvén waves and generation of Alfvén waves via the CR resonant streaming instability, where λ is the wavelength of Alfvén waves, and r_L is the Larmor radius of CRs. For CRs streaming from a source to a sink, when their bulk drift velocity, i.e., streaming velocity v_D , is larger than the Alfvén speed V_A , the Alfvén waves excited by streaming CRs become unstable. The wave growth rate is (Kulsrud & Pearce 1969)

$$\Gamma_{CR} = \Omega_0 \frac{n_{CR>(> r_L)} }{n} \left(\frac{v_D}{V_A} - 1 \right), \quad (1)$$

when neutrals and ions are strongly coupled together with the Alfvén wave frequency $\sim r_L^{-1} V_A$ much smaller than the neutral-ion collisional frequency $\nu_{ni} = \gamma_d \rho_i$ in a weakly ionized medium or the ion-neutral collisional frequency $\nu_{in} = \gamma_d \rho_n$ in a highly ionized medium. Here γ_d is the drag coefficient (Shu 1992), ρ_i and ρ_n are the ion and neutral mass densities, $\Omega_0 = eB_0/(mc)$ is the nonrelativistic gyrofrequency, e and m are the proton electric charge and mass, c is the light speed, $n_{CR>(> r_L)}$ is the number density of CRs with the Larmor radius larger than $r_L \sim \lambda$, n is the total number density of gas, $v_D - V_A$ is the drift velocity in the wave frame, $V_A = B_0/\sqrt{4\pi\rho}$, B_0 is the mean magnetic field strength, and $\rho = \rho_i + \rho_n$ is the total mass density.

When neutrals and ions are weakly coupled with $r_L^{-1} V_{Ai} > \nu_{in}$ in a partially ionized medium, where $V_{Ai} = B_0/\sqrt{4\pi\rho_i}$ is the Alfvén speed in ions, or in a fully ionized medium, the growth rate is

$$\Gamma_{CR} = \Omega_0 \frac{n_{CR>(> r_L)} }{n_i} \left(\frac{v_D}{V_{Ai}} - 1 \right). \quad (2)$$

Here n_i is the ion number density.

The CR-generated Alfvén waves in turn scatter the CRs. The quasilinear gyroresonant scattering of CRs in the wave frame regulates $v_D - V_{A(i)}$. In a steady state, the amplitude of CR-driven Alfvén waves is stabilized by the balance between Γ_{CR} and the damping rate of Alfvén waves. The pitch-angle scattering corresponding to this wave amplitude is also in balance with the net streaming (Kulsrud 2005). The net drift velocity in the wave frame in a steady state is (Kulsrud 2005; Wiener et al. 2013)

$$v_D - V_{A(i)} = \frac{1}{3} v \frac{r_L}{H} \frac{B_0^2}{\delta B(r_L)^2}, \quad (3)$$

where $v \sim c$ for relativistic CRs, H is the distance from the source to the sink, and $\delta B(r_L)^2/B_0^2$ is the relative magnetic fluctuation energy of the resonant Alfvén waves.

The damping of streaming instability depends on both properties of the background MHD turbulence and plasma conditions of the surrounding medium. Next we will discuss different damping mechanisms.

2.2. Turbulent damping

Turbulent damping was first mentioned in Yan & Lazarian (2002) and later studied in detail by Farmer & Goldreich (2004) for trans-Alfvénic turbulence and Lazarian (2016) in various turbulence regimes for a more general astrophysical application. For strong MHD turbulence with the critical balance (Goldreich & Sridhar 1995) between the turbulent motion in the direction perpendicular to the local magnetic field and the wave-like motion along the local magnetic field (Lazarian & Vishniac 1999), i.e.,

$$\frac{x_\perp}{u_x} = \frac{x_\parallel}{V_A}, \quad (4)$$

where x_\perp and x_\parallel are the length scales of a turbulent eddy perpendicular and parallel to the local magnetic field, and

$$u_x = V_{st} (x_\perp / L_{st})^{\frac{1}{3}} \quad (5)$$

is the turbulent velocity at x_\perp . The corresponding turbulent cascading rate, i.e., eddy turnover rate, is

$$u_x x_\perp^{-1} = V_{st} L_{st}^{-\frac{1}{3}} x_\perp^{-\frac{2}{3}}. \quad (6)$$

Here

$$V_{st} = V_A, \quad L_{st} = l_A = LM_A^{-3}, \quad (7)$$

for super-Alfvénic turbulence with the Alfvén Mach number $M_A = V_L/V_A > 1$, l_A is the Alfvénic scale, and

$$V_{st} = V_L M_A, \quad L_{st} = l_{\text{tran}} = LM_A^2, \quad (8)$$

for sub-Alfvénic turbulence with $M_A < 1$, where V_L is the turbulent velocity at the injection scale L of turbulence.

We follow the analysis in Lazarian (2016) to derive the turbulent damping rate. The CR-driven Alfvén waves propagate along the local magnetic field. For the Alfvén waves with the wavelength λ , the distortion by the turbulent motion at the resonant perpendicular scale x_\perp is most efficient. λ and x_\perp are related by

$$\frac{x_\perp}{V_A} = \frac{\lambda}{u_x}. \quad (9)$$

The scaling relations in Eqs. (4) and (9) are illustrated in Fig. 1, and they give

$$\lambda = \frac{u_x}{V_A} x_\perp = \frac{u_x^2}{V_A^2} x_\parallel. \quad (10)$$

By inserting Eq. (5) into Eq. (9), one finds

$$x_\perp = \lambda^{\frac{3}{4}} \left(\frac{V_A}{V_{st}} \right)^{\frac{3}{4}} L_{st}^{\frac{1}{4}}. \quad (11)$$

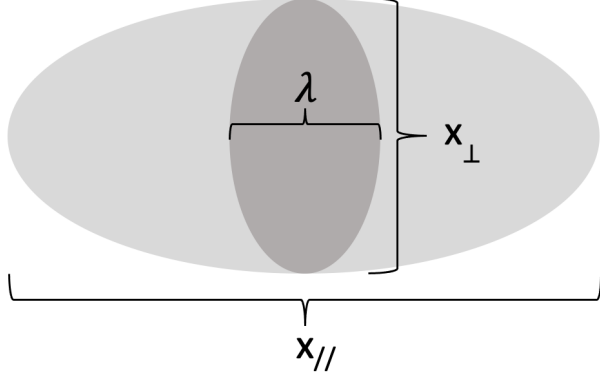


Figure 1. Sketch of the relation between x_{\parallel} and x_{\perp} for strong anisotropic MHD turbulence and the relation between x_{\perp} and λ for turbulent damping of CR-driven Alfvén waves.

The turbulent damping rate is determined by the eddy turnover rate at x_{\perp} (Eqs. (6) and (11)),

$$\Gamma_{st} = \frac{u_x}{x_{\perp}} = V_A^{-\frac{1}{2}} V_{st}^{\frac{3}{2}} L_{st}^{-\frac{1}{2}} \lambda^{-\frac{1}{2}}. \quad (12)$$

Note that x_{\perp} should lie within the range of strong MHD turbulence, i.e., $[x_{\min,\perp}, L_{st}]$, where $x_{\min,\perp}$ is the perpendicular damping scale of MHD turbulence and determined by microscopic plasma effects. The corresponding range of $r_L \sim \lambda$ is (Eq. (11)),

$$\frac{V_{st}}{V_A} L_{st}^{-\frac{1}{3}} x_{\min,\perp}^{\frac{4}{3}} < r_L < \frac{V_{st}}{V_A} L_{st}. \quad (13)$$

Eqs. (12) and (13) become (Eq. (7))

$$\Gamma_{st} = V_A L^{-\frac{1}{2}} M_A^{\frac{3}{2}} \lambda^{-\frac{1}{2}} = V_L L^{-\frac{1}{2}} M_A^{\frac{1}{2}} \lambda^{-\frac{1}{2}}, \quad (14)$$

and

$$l_A^{-\frac{1}{3}} x_{\min,\perp}^{\frac{4}{3}} < r_L < l_A, \quad (15)$$

for super-Alfvénic turbulence, and (Eq. (8))

$$\Gamma_{st} = V_A L^{-\frac{1}{2}} M_A^2 \lambda^{-\frac{1}{2}} = V_L L^{-\frac{1}{2}} M_A \lambda^{-\frac{1}{2}}, \quad (16)$$

and

$$L^{-\frac{1}{3}} M_A^{\frac{4}{3}} x_{\min,\perp}^{\frac{4}{3}} < r_L < L M_A^4, \quad (17)$$

for sub-Alfvénic turbulence. We see that Γ_{st} increases with M_A . Naturally, a larger amplitude of turbulence can result in a more efficient turbulent damping. For the same reason, Γ_{st} of sub-Alfvénic turbulence is smaller than that of super-Alfvénic turbulence under the same physical condition.

2.3. Ion-neutral collisional damping in a partially ionized medium

Alfvén waves propagating in the partially ionized interstellar medium (ISM) with a wide range of ionization fractions, e.g., from weakly ionized molecular clouds (MCs) to highly

ionized warm phases, are subject to the damping effect due to the collisional friction between ions and neutrals.

In a weakly ionized medium with $\nu_{ni} < \nu_{in}$, when ions and neutrals are strongly coupled together with the wave frequency $\omega = V_A k_{\parallel} < \nu_{ni}$, the ion-neutral collisional (IN) damping rate is (Piddington 1956; Kulsrud & Pearce 1969)

$$\Gamma_{IN} = \frac{\xi_n V_A^2 k_{\parallel}^2}{2\nu_{ni}}, \quad (18)$$

where k_{\parallel} is the wavevector component parallel to the magnetic field, and $\xi_n = \rho_n/\rho$. When neutrals and ions are decoupled from each other, i.e., in the weak coupling regime with $\omega = V_A k_{\parallel} > \nu_{in}$, there is

$$\Gamma_{IN} = \frac{\nu_{in}}{2}. \quad (19)$$

MHD turbulent cascade in a weakly ionized medium is also subject to IN damping (Xu et al. 2015, 2016; Xu & Lazarian 2017a). We consider that the driving of turbulence occurs in the strong coupling regime. MHD turbulence is damped when Γ_{IN} in Eq. (18) equalizes with the turbulent cascading rate $u_k k_{\perp}$, where u_k is the turbulent velocity at wavenumber k , and k_{\perp} is the wavevector component perpendicular to the magnetic field. For strong MHD turbulence, k_{\perp} and k_{\parallel} are related by the critical balance relation (see Section 2.2)

$$k_{\perp} u_k = k_{\parallel} V_A. \quad (20)$$

The corresponding IN damping scale of MHD turbulence is (Xu et al. 2015, 2016)

$$x_{\min,\perp} = \left(\frac{2\nu_{ni}}{\xi_n} \right)^{-\frac{3}{2}} L_{st}^{-\frac{1}{2}} V_{st}^{\frac{3}{2}}, \quad (21)$$

which gives the smallest perpendicular scale of MHD turbulent cascade. It becomes

$$x_{\min,\perp} = \left(\frac{2\nu_{ni}}{\xi_n} \right)^{-\frac{3}{2}} L^{-\frac{1}{2}} V_L^{\frac{3}{2}} \quad (22)$$

for super-Alfvénic turbulence, and

$$x_{\min,\perp} = \left(\frac{2\nu_{ni}}{\xi_n} \right)^{-\frac{3}{2}} L^{-\frac{1}{2}} V_L^{\frac{3}{2}} M_A^{\frac{1}{2}} \quad (23)$$

for sub-Alfvénic turbulence. With

$$u_k k_{\perp} = V_A k_{\parallel} < \nu_{ni} < \nu_{in}, \quad (24)$$

and

$$\frac{\xi_n V_A^2 k_{\parallel}^2}{2\nu_{ni}} < \frac{\xi_n \nu_{ni}}{2} < \frac{\nu_{ni}}{2} < \frac{\nu_{in}}{2}, \quad (25)$$

strong MHD turbulence injected in the strong coupling regime cannot cascade into the weak coupling regime, and Γ_{IN} of Alfvén waves in the weak coupling regime is larger than Γ_{IN} and the eddy turnover rate of MHD turbulence in the strong coupling regime (Xu et al. 2016).

In a highly ionized medium with $\nu_{in} < \nu_{ni}$, in the strong coupling regime with $V_A k_{\parallel} < \nu_{in}$, Γ_{IN} is given by Eq. (18). When ions are decoupled from neutrals with $V_A k_{\parallel} > \nu_{in}$, there is (Xu et al. 2016)

$$\Gamma_{IN} = \frac{\nu_{ni} \chi V_{Ai}^2 k_{\parallel}^2}{2[(1 + \chi)^2 \nu_{ni}^2 + V_{Ai}^2 k_{\parallel}^2]}, \quad (26)$$

where $\chi = \rho_n / \rho_i$. When neutrals and ions are decoupled from each other with $V_{Ai} k_{\parallel} > \nu_{ni}$, the above expression can be reduced to Eq. (19). As $u_k k_{\perp} = V_A k_{\parallel}$ (or $V_{Ai} k_{\parallel}$) $> \Gamma_{IN}$ in both strong and weak coupling regimes, MHD turbulence in a highly ionized medium is not damped by IN damping.

Briefly, IN damping is sensitive to the ionization fraction, and the damping effect in a weakly ionized medium is much stronger than that in a highly ionized medium.

2.4. Nonlinear Landau damping

In the fully ionized gaseous Galactic halo or corona (Spitzer 1990; McKee 1993), Alfvén waves are subject to nonlinear Landau (NL) damping due to the resonant interactions of thermal ions with the beat waves produced by couples of Alfvén waves (Lee & Völk 1973; Kulsrud 1978). The damping rate is (Kulsrud 1978)

$$\Gamma_{NL} = \frac{1}{2} \left(\frac{\pi}{2} \right)^{\frac{1}{2}} \frac{v_{th}}{c} \frac{\delta B(r_L)^2}{B_0^2} \Omega, \quad (27)$$

where $\Omega = eB_0 / (\gamma m c) \sim c / r_L$ is the gyrofrequency of relativistic CRs with the Lorentz factor γ , $v_{th} = \sqrt{k_B T_i / m_i}$ is the average thermal ion speed, k_B is the Boltzmann constant, T_i is ion temperature, and m_i is ion mass. Unlike Γ_{st} and Γ_{IN} , Γ_{NL} depends on the amplitude of CR-generated Alfvén waves.

3. TURBULENT DAMPING VS. IN DAMPING

Depending on the driving condition of MHD turbulence and the plasma condition in different interstellar phases, the dominant damping mechanism of streaming instability varies. We first compare turbulent damping with IN damping in weakly and highly ionized media, and then compare turbulent damping with NL damping in a fully ionized hot medium (see Section 4). As the streaming instability and wave damping together determine v_D , a proper description of the damping effect in different regimes is important for determining the diffusion coefficient of CRs and understanding their confinement in the Galaxy.

3.1. Dominant damping mechanism in different regimes

(1) Weakly ionized medium. We first consider the case when both MHD turbulence and CR-driven Alfvén waves are in the strong coupling regime, i.e., $r_L^{-1} V_A < \nu_{ni}$. If the turbulent damping is the dominant damping mechanism, we should have

$$(i): \Gamma_{st}(x_{\perp}) > \Gamma_{IN}(x_{\parallel}), \quad (28)$$

so that MHD turbulence is not damped at x_{\perp} , and

$$(ii): \Gamma_{st}(x_{\perp}) > \Gamma_{IN}(r_L). \quad (29)$$

We easily see

$$r_L < x_{\perp} < x_{\parallel} \quad (30)$$

based on the relation in Eq. (10), meaning

$$\Gamma_{IN}(r_L) > \Gamma_{IN}(x_{\parallel}). \quad (31)$$

Therefore, if condition (ii) is satisfied, then condition (i) is naturally satisfied.

As an example, using the following parameters, we have

$$\begin{aligned} & \frac{V_A}{r_L \nu_{ni}} \\ &= 0.07 \left(\frac{B_0}{1 \mu\text{G}} \right)^2 \left(\frac{n_H}{100 \text{ cm}^{-3}} \right)^{-\frac{3}{2}} \left(\frac{n_e/n_H}{0.1} \right)^{-1} \left(\frac{E_{CR}}{10 \text{ GeV}} \right)^{-1} \\ &< 1, \end{aligned} \quad (32)$$

where n_e/n_H is the ionization fraction, n_e and n_H are number densities of electrons and atomic hydrogen, $m_i = m_n = m_H$, m_n is neutral mass, m_H is hydrogen atomic mass, $\gamma_d = 5.5 \times 10^{14} \text{ cm}^3 \text{ g}^{-1} \text{ s}^{-1}$ (Shu 1992), and E_{CR} is the energy of CR protons. The values used here do not represent the typical conditions of MCs, but are still considered as a possibility given the large variety of interstellar conditions. Condition (ii) in Eq. (29) can be rewritten as (Eqs. (14) and (18))

$$\begin{aligned} M_A &> \left(\frac{\xi_n}{2\nu_{ni}} V_A L^{\frac{1}{2}} r_L^{-\frac{3}{2}} \right)^{\frac{2}{3}} \\ &= 2 \left(\frac{B_0}{1 \mu\text{G}} \right)^{\frac{5}{3}} \left(\frac{n_H}{100 \text{ cm}^{-3}} \right)^{-1} \left(\frac{n_e/n_H}{0.1} \right)^{-\frac{2}{3}} \\ &\quad \left(\frac{L}{0.1 \text{ pc}} \right)^{\frac{1}{3}} \left(\frac{E_{CR}}{10 \text{ GeV}} \right)^{-1} \end{aligned} \quad (33)$$

for super-Alfvénic turbulence driven on small length scales, e.g., near supernova shocks when the shock and shock precursor interact with interstellar or circumstellar density inhomogeneities (e.g., Xu & Lazarian 2017b, 2021). We note that the outer scale of this turbulence is determined by the size of density clumps. For instance, the typical size of ubiquitous HI clouds in the ISM is 0.1 pc (Inoue et al. 2009). As this scale is much larger than r_L of low-energy CRs considered here, the CR-induced Alfvén waves are subject to turbulent damping in this scenario.

With the above parameters used, in Fig. 2(a), the shaded area shows the ranges of M_A and n_e/n_H for turbulent damping to dominate over IN damping. The solid line represents

$$M_A = \left(\frac{\xi_n}{2\nu_{ni}} V_A L^{\frac{1}{2}} r_L^{-\frac{3}{2}} \right)^{\frac{2}{3}}, \quad (34)$$

below which, IN damping dominates over turbulent damping. In the area above the solid line, as MHD turbulence is also subject to IN damping, to ensure that the condition in Eq. (15) is also satisfied, other constraints on M_A indicated in Fig. 2(a) are

$$M_A < \left(\frac{2\nu_{ni}}{\xi_n} \frac{L}{V_A} \right)^{\frac{1}{3}}, \quad (35)$$

corresponding to (Eq. (22))

$$x_{\min,\perp} < l_A, \quad (36)$$

$$M_A < \left[\left(\frac{2\nu_{ni}}{\xi_n} \right)^2 V_A^{-2} L r_L \right]^{\frac{1}{3}}, \quad (37)$$

corresponding to (Eqs. (11) and (22))

$$\Gamma_{st}(x_\perp) > \Gamma_{IN}(x_\parallel), \quad (38)$$

and

$$M_A < \left(\frac{L}{r_L} \right)^{\frac{1}{3}}, \quad (39)$$

corresponding to

$$r_L < l_A. \quad (40)$$

In addition, the vertical dashed line indicates the n_e/n_H value corresponding to $r_L^{-1}V_A = \nu_{ni}$. Toward a larger n_e/n_H , the Alfvén waves are in the strong coupling regime.

In Fig. 2(b), using the M_A value given by Eq. (34), we illustrate the relation between different length scales. For the regime of interest, we have

$$r_{L,\min} < \frac{V_A}{\nu_{ni}} < r_L < x_\perp < x_\parallel < l_A, \quad (41)$$

where $r_{L,\min} = l_A^{-\frac{1}{3}} x_{\min,\perp}^{\frac{4}{3}}$ is given in Eq. (15).

In typical MC conditions, we find that CR-driven Alfvén waves are in the weak coupling regime with

$$\frac{V_{Ai}}{r_L \nu_{in}} \approx 2 \times 10^3 \left(\frac{B_0}{10 \mu\text{G}} \right)^2 \left(\frac{n_H}{100 \text{ cm}^{-3}} \right)^{-\frac{3}{2}} \left(\frac{n_e/n_H}{10^{-4}} \right)^{-\frac{1}{2}} \left(\frac{E_{CR}}{1 \text{ GeV}} \right)^{-1} \gg 1. \quad (42)$$

For MHD turbulence injected at a large scale in the strong coupling regime, there is always (see Section 2.3)

$$\Gamma_{st}(x_\perp) < \Gamma_{IN}(r_L) = \frac{\nu_{in}}{2}. \quad (43)$$

Therefore, the damping of CR-driven Alfvén waves in MCs predominantly comes from ion-neutral collisions.

(2) Highly ionized medium. At a high ionization fraction, when both MHD turbulence and CR-generated Alfvén waves are in the strong coupling regime, i.e., $r_L^{-1}V_A < \nu_{in}$, similar to the analysis for the strong coupling regime in a weakly ionized medium, $\Gamma_{st}(x_\perp)$ should be compared with $\Gamma_{IN}(r_L)$ to determine the relative importance between the two damping effects. When MHD turbulence at x_\perp is in the strong coupling regime, but CR-generated Alfvén waves are in the weak coupling regime and also have $r_L^{-1}V_{Ai} > \nu_{ni}$, IN damping is more important than turbulent damping. When MHD turbulence at x_\perp is also in the weak coupling regime, there is always

$$\Gamma_{st}(x_\perp) > \Gamma_{IN}(r_L) = \frac{\nu_{in}}{2}, \quad (44)$$

and MHD turbulence dominates the wave damping.

By using the typical parameters of the warm ionized medium (WIM) (Reynolds 1992), we find that CR-generated Alfvén waves are in the weak coupling regime and further have

$$\frac{V_{Ai}}{r_L \nu_{ni}} = 7.6 \times 10^3 \left(\frac{B_0}{1 \mu\text{G}} \right)^2 \left(\frac{n_i}{0.1 \text{ cm}^{-3}} \right)^{-\frac{3}{2}} \left(\frac{E_{CR}}{1 \text{ GeV}} \right)^{-1} \gg 1. \quad (45)$$

As discussed above, under the condition

$$\frac{\Gamma_{st}(x_\perp)}{\Gamma_{IN}(r_L)} = \frac{\Gamma_{st}(x_\perp)}{\frac{\nu_{in}}{2}} > 1, \quad (46)$$

turbulent damping dominates over IN damping. The above condition can be rewritten as (Eq. (14))

$$M_A > \left(\frac{\nu_{in}}{2} V_{Ai}^{-1} L^{\frac{1}{2}} r_L^{\frac{1}{2}} \right)^{\frac{2}{3}} = 0.2 \left(\frac{B_0}{1 \mu\text{G}} \right)^{-1} \left(\frac{n_i}{0.1 \text{ cm}^{-3}} \right)^{\frac{1}{3}} \left(\frac{n_n}{0.01 \text{ cm}^{-3}} \right)^{\frac{2}{3}} \left(\frac{L}{100 \text{ pc}} \right)^{\frac{1}{3}} \left(\frac{E_{CR}}{1 \text{ GeV}} \right)^{\frac{1}{3}} \quad (47)$$

for super-Alfvénic turbulence, which is naturally satisfied, and (Eq. (16))

$$M_A > \left(\frac{\nu_{in}}{2} V_{Ai}^{-1} L^{\frac{1}{2}} r_L^{\frac{1}{2}} \right)^{\frac{1}{2}} = 0.3 \left(\frac{B_0}{1 \mu\text{G}} \right)^{-\frac{3}{4}} \left(\frac{n_i}{0.1 \text{ cm}^{-3}} \right)^{\frac{1}{4}} \left(\frac{n_n}{0.01 \text{ cm}^{-3}} \right)^{\frac{1}{2}} \left(\frac{L}{100 \text{ pc}} \right)^{\frac{1}{4}} \left(\frac{E_{CR}}{1 \text{ GeV}} \right)^{\frac{1}{4}} \quad (48)$$

for sub-Alfvénic turbulence, where n_n is the neutral number density, and $L \sim 100 \text{ pc}$ is the typical injection scale of interstellar turbulence driven by supernova explosions. We note that $V_A \approx V_{Ai}$ can be used for estimating M_A of MHD turbulence injected in the strong coupling regime in a highly ionized medium. As the above constraints on M_A can be easily satisfied in the WIM, turbulent damping is likely to be the dominant damping effect for CR-generated Alfvén waves in the WIM.

3.2. v_D in different regimes

Knowing the dominant damping mechanism in different coupling regimes and at different ionization fractions, we can further determine v_D at the balance between wave growth and damping.

(1) Weakly ionized medium. In the strong coupling regime, when MHD turbulence dominates the wave damping, at the balance between growth and damping rates of Alfvén waves (Eqs. (1) and (12)), we find

$$\frac{v_D}{V_A} = 1 + \Omega_0^{-1} \left(\frac{n_{CR}(> r_L)}{n} \right)^{-1} V_A^{-\frac{1}{2}} V_{st}^{\frac{3}{2}} L^{-\frac{1}{2}} r_L^{-\frac{1}{2}}, \quad (49)$$

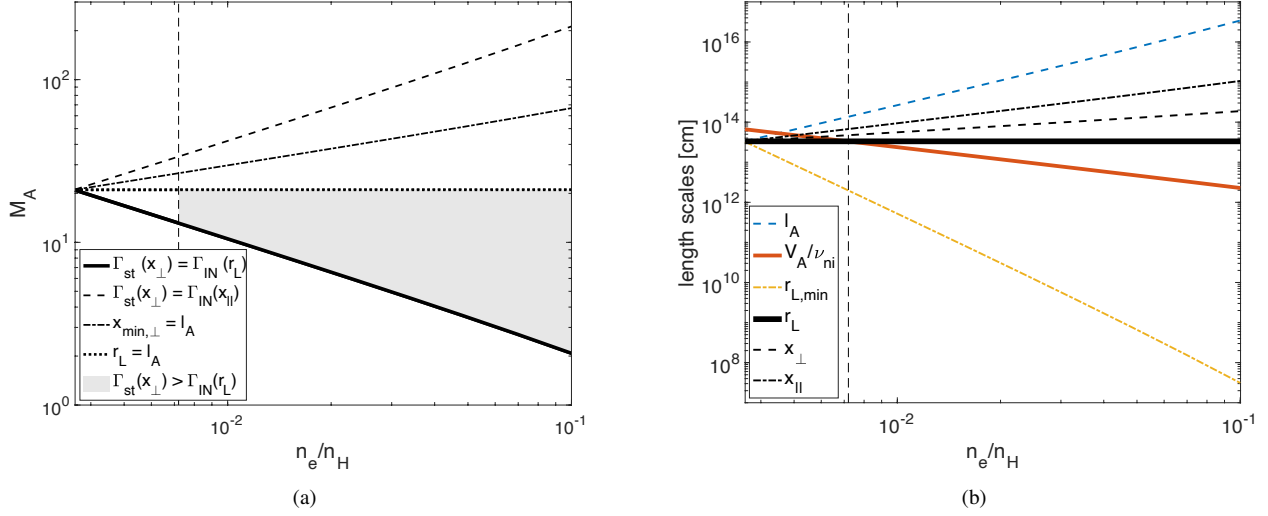


Figure 2. (a) Ranges of M_A and n_e/n_H for turbulent damping to dominate over IN damping (shaded area above the solid line) and for IN damping to dominate over turbulent damping (below the solid line) in a weakly ionized medium, where super-Alfvénic turbulence driven on a small length scale (0.1 pc) is considered. Other limits on M_A are indicated by other lines as explained in the text. (b) Relation between different length scales, where the M_A value corresponding to the solid line in (a) is used. The vertical dashed lines in (a) and (b) correspond to $r_L^{-1}V_A = \nu_{ni}$ with $n_e/n_H = 0.007$.

which is (Eq. (7))

$$\frac{v_D}{V_A} \approx 1 + 1.7 \times 10^5 \left(\frac{B_0}{1 \mu\text{G}} \right)^{-1} \left(\frac{n_H}{100 \text{ cm}^{-3}} \right)^{\frac{5}{4}} \left(\frac{L}{0.1 \text{ pc}} \right)^{-\frac{1}{2}} \left(\frac{V_L}{1 \text{ km s}^{-1}} \right)^{\frac{3}{2}} \left(\frac{E_{CR}}{10 \text{ GeV}} \right)^{1.1} \quad (50)$$

for super-Alfvénic turbulence, where we adopt the integral number density of CRs near the Sun (Wentzel 1974)

$$n_{CR>(> r_L)} = 2 \times 10^{-10} \gamma^{-1.6} \text{ cm}^{-3}. \quad (51)$$

When ion-neutral collisions dominate the wave damping, there is (Eqs. (1) and (18))

$$\frac{v_D}{V_A} = 1 + \Omega_0^{-1} \left(\frac{n_{CR>(> r_L)}{n} \right)^{-1} \frac{\xi_n V_A^2 r_L^{-2}}{2\nu_{ni}} \approx 1 + 4.9 \times 10^4 \left(\frac{B_0}{1 \mu\text{G}} \right)^3 \left(\frac{n_H}{100 \text{ cm}^{-3}} \right)^{-1} \left(\frac{n_e/n_H}{0.1} \right)^{-1} \left(\frac{E_{CR}}{10 \text{ GeV}} \right)^{-0.4}. \quad (52)$$

We see that with the parameters adopted here, in the strong coupling regime there is $v_D \gg V_A$ due to the strong damping of CR-generated Alfvén waves irrespective of the dominant damping mechanism.

In a typical MC environment, when CR-driven Alfvén waves are in the weak coupling regime and mainly subject

to IN damping, we have (Eqs. (2) and (19))

$$\frac{v_D}{V_{Ai}} = 1 + \frac{\nu_{in}}{2} \Omega_0^{-1} \left(\frac{n_{CR>(> r_L)}{n_i} \right)^{-1} \approx 1 + 26.5 \left(\frac{B_0}{10 \mu\text{G}} \right)^{-1} \left(\frac{n_H}{100 \text{ cm}^{-3}} \right)^2 \left(\frac{n_e/n_H}{10^{-4}} \right) \left(\frac{E_{CR}}{1 \text{ GeV}} \right)^{1.6}. \quad (53)$$

We see that v_D is significantly larger than V_{Ai} due to the damping effect.

(2) Highly ionized medium. In the WIM, CR-driven Alfvén waves are in the weak coupling regime and mainly subject to turbulent damping. $\Gamma_{CR} = \Gamma_{st}$ gives (Eqs. (2), (7), (8), (12))

$$\frac{v_D}{V_{Ai}} = 1 + \Omega_0^{-1} \left(\frac{n_{CR>(> r_L)}{n_i} \right)^{-1} V_{Ai}^{-\frac{1}{2}} V_{st}^{\frac{3}{2}} L_{st}^{-\frac{1}{2}} r_L^{-\frac{1}{2}} \approx 1 + 3.2 \left(\frac{B_0}{1 \mu\text{G}} \right)^{-1} \left(\frac{n_i}{0.1 \text{ cm}^{-3}} \right)^{\frac{5}{4}} \left(\frac{E_{CR}}{1 \text{ GeV}} \right)^{1.1} \left(\frac{V_L}{10 \text{ km s}^{-1}} \right)^{\frac{3}{2}} \left(\frac{L}{100 \text{ pc}} \right)^{-\frac{1}{2}} \quad (54)$$

for super-Alfvénic turbulence, and

$$\frac{v_D}{V_{Ai}} \approx 1 + 0.9 \left(\frac{B_0}{1 \mu\text{G}} \right)^{-\frac{3}{2}} \left(\frac{n_i}{0.1 \text{ cm}^{-3}} \right)^{\frac{3}{2}} \left(\frac{E_{CR}}{1 \text{ GeV}} \right)^{1.1} \left(\frac{V_L}{5 \text{ km s}^{-1}} \right)^2 \left(\frac{L}{100 \text{ pc}} \right)^{-\frac{1}{2}} \quad (55)$$

for sub-Alfvénic turbulence, where we consider $V_A \approx V_{Ai}$ and $n_i \approx n_H$, and $V_L \sim 10 \text{ km s}^{-1}$ is the typical turbulent velocity for supernova-driven turbulence (Chamandy &

Shukurov 2020). The second term in Eqs. (54) and (55) becomes the dominant term at higher CR energies, and v_D is energy dependent. The larger v_D in Eq. (54) is caused by the stronger turbulent damping in super-Alfvénic turbulence than in sub-Alfvénic turbulence (see Section 2.2).

3.3. Diffusion coefficient in different regimes

The diffusion coefficient D of streaming CRs depends on both v_D and the characteristic scale of turbulent magnetic fields. In super-Alfvénic turbulence, l_A is the characteristic tangling scale of turbulent magnetic fields, at which the turbulent and magnetic energies are in equipartition. Over l_A the field line changes its orientation in a random walk manner. Therefore, l_A is the effective mean free path of CRs streaming along turbulent magnetic field lines (Brunetti & Lazarian 2007). In sub-Alfvénic turbulence, magnetic fields are weakly perturbed with an insignificant change of magnetic field orientation on all length scales. So the magnetic field structure cannot provide additional confinement for streaming CRs. In this case, streaming CRs do not have a diffusive propagation in the observer frame, but we still introduce a diffusion coefficient to quantify the CR confinement and adopt the CR gradient scale length H for calculating D .

In a weakly ionized medium, e.g., MCs, by using Eq. (53) and considering super-Alfvénic turbulence, we have

$$D = v_D l_A = V_{Ai} \frac{v_D}{V_{Ai}} L M_A^{-3} \approx 1.8 \times 10^{28} \text{ cm}^2 \text{ s}^{-1} \left(\frac{n_H}{100 \text{ cm}^{-3}} \right)^{\frac{3}{2}} \left(\frac{n_e/n_H}{10^{-4}} \right)^{\frac{1}{2}} \left(\frac{E_{CR}}{1 \text{ GeV}} \right)^{1.6} \left(\frac{L}{10 \text{ pc}} \right) M_A^{-3}, \quad (56)$$

where the factor M_A^{-3} can be much smaller than unity. Here we consider $L \sim 10$ pc for turbulence in MCs, and we note that as MHD turbulence is in the strong coupling regime, V_A should be used when calculating M_A . As $D \propto M_A^{-3}$, a slow diffusion with a small D is expected at a large M_A .

In a highly ionized medium, e.g., the WIM, we have

$$D = v_D l_A \quad (57)$$

for super-Alfvénic turbulence, and

$$D = v_D H \quad (58)$$

for sub-Alfvénic turbulence, where v_D is given in Eq. (54) and Eq. (55), respectively, and $H \sim 1$ kpc as the scale height of the WIM. In Fig. 3, we present D as a function of E_{CR} for both super- and sub-Alfvénic turbulence with $M_A = 1.4$ and 0.7 in the WIM. The smaller D in super-Alfvénic turbulence is caused by the tangling of turbulent magnetic fields. We see $D \propto E_{CR}^{1.1}$ in both turbulence regimes. This steep energy scaling can be important for explaining the CR spectrum observed at Earth below ~ 100 GeV (Blasi et al. 2012).

4. TURBULENT DAMPING VS. NL DAMPING

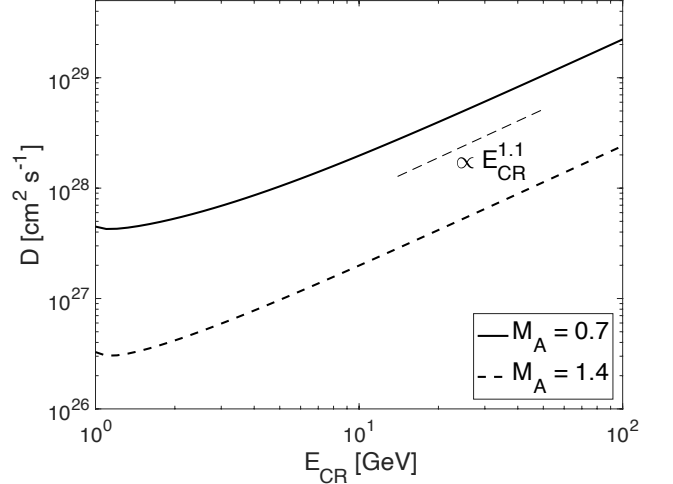


Figure 3. Diffusion coefficient vs. E_{CR} in super- and sub-Alfvénic turbulence in the WIM.

In the Galactic halo, if NL damping is the dominant damping mechanism of CR-generated Alfvén waves, at the balance

$$\Gamma_{CR} = \Gamma_{NL}, \quad (59)$$

by combining Eqs. (2), (3), and (27), one can obtain

$$v_D = V_{Ai} + \frac{\sqrt{c}}{3} H^{-\frac{1}{2}} \left[\frac{2}{3} \sqrt{\frac{2}{\pi}} \frac{\Omega_0}{v_{th}} \frac{n_{CR}(> r_L)}{n_i} \frac{1}{V_{Ai}} \right]^{-\frac{1}{2}}, \quad (60)$$

and

$$\frac{\delta B(r_L)^2}{B_0^2} = \left[\frac{2}{3} \sqrt{\frac{2}{\pi}} \frac{\Omega_0}{v_{th}} \frac{n_{CR}(> r_L)}{n_i} \frac{c}{V_{Ai}} \frac{r_L^2}{H} \right]^{\frac{1}{2}}. \quad (61)$$

Inserting Eq. (61) into Eq. (27) yields

$$\Gamma_{NL} = \left(\frac{\pi}{2} \right)^{\frac{1}{4}} \left(\frac{1}{6} \right)^{\frac{1}{2}} v_{th}^{\frac{1}{2}} \left[\Omega_0 \frac{n_{CR}(> r_L)}{n_i} \frac{c}{V_{Ai}} \frac{1}{H} \right]^{\frac{1}{2}}, \quad (62)$$

which becomes smaller at a larger H with a smaller CR gradient. To be consistent with our assumption that NL damping dominates over turbulent damping, the condition (Eqs. (12) and (62))

$$\frac{\Gamma_{NL}}{\Gamma_{st}} = \left[\left(\frac{\pi}{2} \right)^{\frac{1}{2}} \frac{1}{6} \frac{L_{st}}{H} \frac{n_{CR}(> r_L)}{n_i} \frac{v_{th}}{V_{st}} \frac{c}{V_{st}} \frac{\Omega_0 r_L}{V_{st}} \right]^{\frac{1}{2}} > 1 \quad (63)$$

should be satisfied.

If turbulent damping dominates over NL damping, the balance (Eqs. (2) and (12))

$$\Gamma_{CR} = \Gamma_{st} \quad (64)$$

gives (see also Eq. (54))

$$v_D = V_{Ai} + \Omega_0^{-1} \left(\frac{n_{CR}(> r_L)}{n_i} \right)^{-1} V_{Ai}^{\frac{1}{2}} V_{st}^{\frac{3}{2}} L_{st}^{-\frac{1}{2}} r_L^{-\frac{1}{2}}. \quad (65)$$

Then inserting the above expression into Eq. (3) gives

$$\frac{\delta B(r_L)^2}{B_0^2} = \frac{c}{3H} \Omega_0 \frac{n_{CR}(> r_L)}{n_i} V_{Ai}^{-\frac{1}{2}} V_{st}^{-\frac{3}{2}} L_{st}^{\frac{1}{2}} r_L^{\frac{3}{2}}. \quad (66)$$

Moreover, Γ_{NL} corresponding to the above relative magnetic fluctuation energy is (Eqs. (27) and (66))

$$\Gamma_{NL} = \frac{1}{6} \left(\frac{\pi}{2}\right)^{\frac{1}{2}} \frac{c}{H} \Omega_0 v_{th} \frac{n_{CR}(> r_L)}{n_i} V_{Ai}^{-\frac{1}{2}} V_{st}^{-\frac{3}{2}} r_L^{\frac{1}{2}} L_{st}^{\frac{1}{2}}. \quad (67)$$

Under the assumption of dominant turbulent damping, there should be

$$\frac{\Gamma_{NL}}{\Gamma_{st}} = \left(\frac{\pi}{2}\right)^{\frac{1}{2}} \frac{1}{6} \frac{L_{st}}{H} \frac{n_{CR}(> r_L)}{n_i} \frac{v_{th}}{V_{st}} \frac{c}{V_{st}} \frac{\Omega_0 r_L}{V_{st}} < 1. \quad (68)$$

Comparing the conditions in Eqs. (63) and (68), we see that at $\Gamma_{NL} = \Gamma_{st}$, there is

$$\left(\frac{\pi}{2}\right)^{\frac{1}{2}} \frac{1}{6} \frac{L_{st}}{H} \frac{n_{CR}(> r_L)}{n_i} \frac{v_{th}}{V_{st}} \frac{c}{V_{st}} \frac{\Omega_0 r_L}{V_{st}} = 1. \quad (69)$$

Using the typical parameters in the Galactic halo (Farmer & Goldreich 2004), we find that the turbulence in this low-density environment has

$$M_A \approx 0.1 \left(\frac{V_L}{10 \text{ km s}^{-1}}\right) \left(\frac{B_0}{1 \mu\text{G}}\right)^{-1} \left(\frac{n_i}{10^{-3} \text{ cm}^{-3}}\right)^{\frac{1}{2}}. \quad (70)$$

For sub-Alfvénic turbulence, Eq. (69) can be rewritten as

$$M_A = \left[\left(\frac{\pi}{2}\right)^{\frac{1}{2}} \frac{1}{6} \frac{L}{H} \frac{n_{CR}(> r_L)}{n_i} \frac{v_{th}}{V_{Ai}} \frac{c}{V_{Ai}} \frac{\Omega_0 r_L}{V_{Ai}} \right]^{\frac{1}{4}}, \quad (71)$$

which is shown as the solid line in Fig. 4. Other parameters are $T_i = 10^6$ K, $L = 100$ pc, and $E_{CR} = 1$ GeV. The area above and below the solid line corresponds to the parameter space for turbulent damping and NL damping to be the dominant damping mechanism, respectively. When turbulent damping is dominant, another constraint on M_A is (Eq. (17))

$$M_A > \left(\frac{r_L}{L}\right)^{\frac{1}{4}} \approx 0.008, \quad (72)$$

which is naturally satisfied in this situation.

Given the small M_A of MHD turbulence in the Galactic halo, the wave damping is more likely to be dominated by NL damping. Using Eq. (60), we find

$$\frac{v_D}{V_{Ai}} \approx 1 + 0.02 \left(\frac{H}{5 \text{ kpc}}\right)^{-\frac{1}{2}} \left(\frac{B_0}{1 \mu\text{G}}\right)^{-1} \left(\frac{n_i}{10^{-3} \text{ cm}^{-3}}\right)^{\frac{3}{4}} \left(\frac{T_i}{10^6 \text{ K}}\right)^{\frac{1}{4}} \left(\frac{E_{CR}}{1 \text{ GeV}}\right)^{0.8}. \quad (73)$$

v_D is very close to V_{Ai} , indicative of the insignificant wave damping in the Galactic halo. Therefore, GeV CRs can be confined due to streaming instability. For CRs with $E_{CR} <$

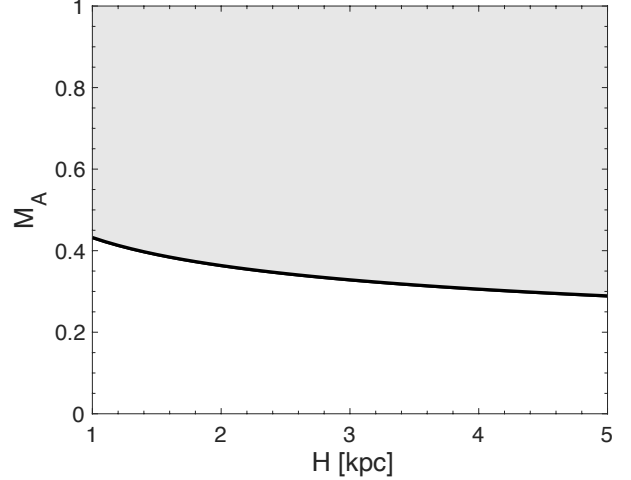


Figure 4. Comparison between turbulent damping and NL damping for Alfvén waves generated by GeV CRs in the Galactic halo. The shaded area shows the ranges of M_A and H for turbulent damping to dominate over NL damping. The solid line represents the relation in Eq. (71).

100 GeV, there is approximately

$$D \approx V_{Ai} H = 1.1 \times 10^{29} \text{ cm}^2 \text{ s}^{-1} \left(\frac{B_0}{1 \mu\text{G}}\right) \left(\frac{n_i}{10^{-3} \text{ cm}^{-3}}\right)^{-\frac{1}{2}} \left(\frac{H}{5 \text{ kpc}}\right), \quad (74)$$

which is energy independent.

5. DISCUSSION

Effect of MHD turbulence on diffusion of streaming CRs.

In cases when MHD turbulence dominates the damping of streaming instability, e.g., in the WIM, MHD turbulence is important for setting v_D . Super-Alfvénic turbulence also provides additional confinement to streaming CRs due to the field line tangling at l_A , irrespective of the dominant damping mechanism. In addition, the non-resonant mirroring interaction of CRs with slow and fast modes in MHD turbulence can also suppress the diffusion of CRs in the vicinity of CR sources (Lazarian & Xu 2021; Xu 2021). The relative importance between mirroring and streaming instability in affecting CR diffusion near CR sources will be investigated in our future work. In this work we do not consider gyroreso-

nant scattering and resonance-broadened transit time damping (TTD) by fast modes of MHD turbulence (Xu & Lazarian 2018, 2020), as fast modes are damped at a large scale due to IN damping in a weakly ionized medium (Xu et al. 2016) and their energy fraction is small at a small M_A (Hu et al. 2021). Moreover, the energy scaling of diffusion coefficient corresponding to scattering by fast modes is incompatible with AMS-02 observations at CR energies $\lesssim 10^3$ GeV (Kempski & Quataert 2021).

Cutoff range of Alfvén waves in a weakly ionized medium. In a weakly ionized medium, within the cutoff range of k_{\parallel} there is no propagation of Alfvén waves due to the severe IN damping (Kulsrud & Pearce 1969). The boundary $[k_{c,\parallel}^+, k_{c,\parallel}^-]$ of the cutoff range is set by $\omega = \Gamma_{IN}$ in both strong and weak coupling regimes (Xu et al. 2015),

$$k_{c,\parallel}^+ = \frac{2\nu_{ni}}{V_A \xi_n}, \quad k_{c,\parallel}^- = \frac{\nu_{in}}{2V_{Ai}}. \quad (75)$$

If CR-driven Alfvén waves fall in the cutoff range with

$$k_{c,\parallel}^+ < r_L^{-1} < k_{c,\parallel}^-, \quad (76)$$

the streaming instability cannot occur. We note that for GeV CRs in a typical MC environment, the CR-driven Alfvén waves are in the weak coupling regime with $r_L^{-1} \gg k_{c,\parallel}^-$ (see Eq. (42)).

Microscopic vs. macroscopic diffusion. By “microscopic diffusion”, we refer to the diffusion in the wave frame caused by the gyroresonant scattering of CRs by CR-amplified Alfvén waves, while the “macroscopic diffusion” in the observer frame is a result of both streaming of CRs and tangling of turbulent magnetic fields on scales much larger than r_L . The former was included in calculating the total diffusion coefficient in earlier studies, e.g., Hopkins et al. (2021). In this work we only consider the latter as it can be directly compared with observations in the observer frame, which was also adopted in Krumholz et al. (2020) for studying CR transport in starburst galaxies.

Coupling between CRs and gas. In the Galactic disk with super-Alfvénic turbulence (Hu et al. 2019), due to the strong IN damping and turbulent damping, CRs have fast streaming and do not suffer significant energy loss via wave generation. The coupling between CRs and gas is caused by field line tangling. This coupling can result in additional pressure support and suppression of star formation. By contrast, in the Galactic halo with sub-Alfvénic turbulence, due to the weak NL damping, CRs are well self-confined and coupled to the gas via streaming instability, and thus effectively transfer momentum to the gas. Both wave damping and turbulent tangling can significantly affect the transport of streaming CRs and their coupling with the gas, and thus are important for studying CR-driven galactic winds.

Turbulence and CRs at phase transition. In the multi-phase ISM, the transition from hot/warm to cold gas can be driven by, e.g., passage of shock waves (Inutsuka et al. 2015). The phase transition induces various instabilities and turbulence.

The turbulent mixing layers at the interfaces between different gas phases have been recently studied in detail by Ji et al. (2019). As the transport of CRs is sensitive to the turbulent magnetic field structure, when CRs interact with the shock-compressed magnetic field, they can be reflected off the shock surface (Xu & Lazarian 2021) and undergo an abrupt change of trajectory.

6. SUMMARY

We study the damping of streaming instability of GeV-100 GeV CRs and the resulting diffusion coefficients in different MHD turbulence regimes and interstellar phases.

In a partially ionized medium, both CR-generated Alfvén waves and MHD turbulence are subject to IN damping. The damping rate depends on the ionization fraction and the coupling state between ions and neutrals. In both weakly ionized MCs and highly ionized WIM, CR-generated Alfvén waves are in the weak coupling regime. In a weakly ionized medium, IN damping is strong and dominates the damping of both MHD turbulence and CR-amplified Alfvén waves. In a highly ionized medium, IN damping is so weak that MHD turbulence injected in the strong coupling regime can cascade into the weak coupling regime and dominates the wave damping.

Both IN damping in MCs and turbulent damping in the WIM act to suppress the streaming instability, leading to a streaming speed of CRs larger than the Alfvén speed. The resulting diffusion coefficient is thus dependent on CR energies. The steep energy scaling of diffusion coefficient in the WIM (see Fig. 3) is important for explaining the CR spectrum observed at Earth, as the turbulence properties measured in the nearby ($\lesssim 1$ kpc) ISM (Armstrong et al. 1995) are similar to that in the WIM (Chepurnov & Lazarian 2010).

We find that MHD turbulence not only can affect the CR streaming speed by turbulent damping but also causes the diffusive propagation of streaming CRs by the field line tangling. The latter effect was not considered in most earlier studies on CR streaming. Because of the field line tangling in super-Alfvénic turbulence at $l_A = LM_A^{-3}$, CRs streaming along turbulent field lines have an effective mean free path given by l_A . At a large M_A in, e.g., cold interstellar phases, a significant reduction of the diffusion coefficient by M_A^{-3} is expected. The slow diffusion of streaming CRs in star-forming MCs can have an important influence on the Galactic disk structure and star formation (Semenov et al. 2021). In the multi-phase ISM with a large variety of M_A of interstellar turbulence, measuring M_A with new techniques (e.g., Lazarian et al. 2018; Xu & Hu 2021) is necessary for realistic modeling of diffusion coefficients of streaming CRs.

In the diffuse Galactic halo, MHD turbulence is sub-Alfvénic with a small M_A , and NL damping is a more important mechanism for damping CR-generated Alfvén waves. This finding is different from that in Lazarian (2016). The resulting streaming speed is basically given by Alfvén speed, and CRs are confined mainly due to streaming instability. In the WIM and Galactic halo, the global pressure gradient formed by streaming CRs plays an important dynamical role

in driving galactic outflows and affecting galaxy evolution (Padovani et al. 2020).

In addition to the interstellar turbulence injected on $\sim 10 - 100$ pc, we also considered a special case with small-scale ($\lesssim 0.1$ pc) preshock turbulence in supernova remnants, which is driven by the interaction between the CR precursor and upstream density inhomogeneities. When CR-amplified Alfvén waves are in the strong coupling regime at a low ionization fraction, we find the condition and parameter space for turbulent damping to dominate over IN damping of streaming instability.

ACKNOWLEDGMENTS

S.X. acknowledges the support for this work provided by NASA through the NASA Hubble Fellowship grant # HST-HF2-51473.001-A awarded by the Space Telescope Science Institute, which is operated by the Association of Universities for Research in Astronomy, Incorporated, under NASA contract NAS5-26555. A.L. acknowledges the support of NASA ATP AAH7546.

Software: MATLAB (MATLAB 2021)

REFERENCES

- Amato, E., & Casanova, S. 2021, *Journal of Plasma Physics*, 87, 845870101, doi: [10.1017/S0022377821000064](https://doi.org/10.1017/S0022377821000064)
- Armillotta, L., Ostriker, E. C., & Jiang, Y.-F. 2021, *ApJ*, 922, 11, doi: [10.3847/1538-4357/ac1db2](https://doi.org/10.3847/1538-4357/ac1db2)
- Armstrong, J. W., Rickett, B. J., & Spangler, S. R. 1995, *ApJ*, 443, 209, doi: [10.1086/175515](https://doi.org/10.1086/175515)
- Bell, A. R. 1978, *MNRAS*, 182, 147, doi: [10.1093/mnras/182.2.147](https://doi.org/10.1093/mnras/182.2.147)
- Blasi, P., Amato, E., & Serpico, P. D. 2012, *PhRvL*, 109, 061101, doi: [10.1103/PhysRevLett.109.061101](https://doi.org/10.1103/PhysRevLett.109.061101)
- Brunetti, G., & Jones, T. W. 2014, *International Journal of Modern Physics D*, 23, 1430007, doi: [10.1142/S0218271814300079](https://doi.org/10.1142/S0218271814300079)
- Brunetti, G., & Lazarian, A. 2007, *MNRAS*, 378, 245, doi: [10.1111/j.1365-2966.2007.11771.x](https://doi.org/10.1111/j.1365-2966.2007.11771.x)
- Chamandy, L., & Shukurov, A. 2020, *Galaxies*, 8, 56, doi: [10.3390/galaxies8030056](https://doi.org/10.3390/galaxies8030056)
- Chepurnov, A., & Lazarian, A. 2010, *ApJ*, 710, 853, doi: [10.1088/0004-637X/710/1/853](https://doi.org/10.1088/0004-637X/710/1/853)
- Farmer, A. J., & Goldreich, P. 2004, *ApJ*, 604, 671, doi: [10.1086/382040](https://doi.org/10.1086/382040)
- Goldreich, P., & Sridhar, S. 1995, *ApJ*, 438, 763, doi: [10.1086/175121](https://doi.org/10.1086/175121)
- Guo, F., & Oh, S. P. 2008, *MNRAS*, 384, 251, doi: [10.1111/j.1365-2966.2007.12692.x](https://doi.org/10.1111/j.1365-2966.2007.12692.x)
- Holguin, F., Ruszkowski, M., Lazarian, A., Farber, R., & Yang, H. Y. K. 2019, *MNRAS*, 490, 1271, doi: [10.1093/mnras/stz2568](https://doi.org/10.1093/mnras/stz2568)
- Hopkins, P. F., Squire, J., Chan, T. K., et al. 2021, *MNRAS*, 501, 4184, doi: [10.1093/mnras/staa3691](https://doi.org/10.1093/mnras/staa3691)
- Hu, Y., Lazarian, A., & Xu, S. 2021, arXiv:2111.15066, arXiv:2111.15066. <https://arxiv.org/abs/2111.15066>
- Hu, Y., Yuen, K. H., Lazarian, V., et al. 2019, *Nature Astronomy*, 3, 776, doi: [10.1038/s41550-019-0769-0](https://doi.org/10.1038/s41550-019-0769-0)
- Inoue, T., Yamazaki, R., & Inutsuka, S.-i. 2009, *ApJ*, 695, 825, doi: [10.1088/0004-637X/695/2/825](https://doi.org/10.1088/0004-637X/695/2/825)
- Inutsuka, S. i., Inoue, T., Iwasaki, K., et al. 2015, in *Astronomical Society of the Pacific Conference Series*, Vol. 498, *Numerical Modeling of Space Plasma Flows ASTRONOM-2014*, ed. N. V. Pogorelov, E. Audit, & G. P. Zank, 75
- Ipavich, F. M. 1975, *ApJ*, 196, 107, doi: [10.1086/153397](https://doi.org/10.1086/153397)
- Ji, S., Oh, S. P., & Masterson, P. 2019, *MNRAS*, 487, 737, doi: [10.1093/mnras/stz1248](https://doi.org/10.1093/mnras/stz1248)
- Kempski, P., & Quataert, E. 2021, arXiv:2109.10977, arXiv:2109.10977. <https://arxiv.org/abs/2109.10977>
- Krumholz, M. R., Crocker, R. M., Xu, S., et al. 2020, *MNRAS*, 493, 2817, doi: [10.1093/mnras/staa493](https://doi.org/10.1093/mnras/staa493)
- Kulsrud, R., & Pearce, W. P. 1969, *ApJ*, 156, 445, doi: [10.1086/149981](https://doi.org/10.1086/149981)
- Kulsrud, R. M. 1978, in *Astronomical Papers Dedicated to Bengt Stromgren*, ed. A. Reiz & T. Andersen, 317–326
- Kulsrud, R. M. 2005, *Plasma physics for astrophysics*, ed. R. M. Kulsrud
- Lazarian, A. 2006, *ApJL*, 645, L25, doi: [10.1086/505796](https://doi.org/10.1086/505796)

- . 2016, *ApJ*, 833, 131, doi: [10.3847/1538-4357/833/2/131](https://doi.org/10.3847/1538-4357/833/2/131)
- Lazarian, A., & Vishniac, E. T. 1999, *ApJ*, 517, 700, doi: [10.1086/307233](https://doi.org/10.1086/307233)
- Lazarian, A., & Xu, S. 2021, submitted to *ApJ*
- Lazarian, A., Yuen, K. H., Ho, K. W., et al. 2018, *ApJ*, 865, 46, doi: [10.3847/1538-4357/aad7ff](https://doi.org/10.3847/1538-4357/aad7ff)
- Lee, M. A., & Völk, H. J. 1973, *Ap&SS*, 24, 31, doi: [10.1007/BF00648673](https://doi.org/10.1007/BF00648673)
- Mao, S. A., & Ostriker, E. C. 2018, *ApJ*, 854, 89, doi: [10.3847/1538-4357/aaa88e](https://doi.org/10.3847/1538-4357/aaa88e)
- Marcowith, A., van Marle, A. J., & Plotnikov, I. 2021, *Physics of Plasmas*, 28, 080601, doi: [10.1063/5.0013662](https://doi.org/10.1063/5.0013662)
- MATLAB. 2021, MATLAB and Statistics Toolbox Release 2021b (Natick, Massachusetts: The MathWorks Inc.)
- McKee, C. F. 1993, in *American Institute of Physics Conference Series*, Vol. 278, *Back to the Galaxy*, ed. S. S. Holt & F. Verter, 499–513, doi: [10.1063/1.43978](https://doi.org/10.1063/1.43978)
- Padovani, M., Ivlev, A. V., Galli, D., et al. 2020, *SSRv*, 216, 29, doi: [10.1007/s11214-020-00654-1](https://doi.org/10.1007/s11214-020-00654-1)
- Piddington, J. H. 1956, *MNRAS*, 116, 314
- Plotnikov, I., Ostriker, E. C., & Bai, X.-N. 2021, *ApJ*, 914, 3, doi: [10.3847/1538-4357/abf7b3](https://doi.org/10.3847/1538-4357/abf7b3)
- Quataert, E., Jiang, Y.-F., & Thompson, T. A. 2021, *MNRAS*, doi: [10.1093/mnras/stab3274](https://doi.org/10.1093/mnras/stab3274)
- Reynolds, R. J. 1992, in *American Institute of Physics Conference Series*, Vol. 278, *American Institute of Physics Conference Series*, 156–165, doi: [10.1063/1.44005](https://doi.org/10.1063/1.44005)
- Semenov, V. A., Kravtsov, A. V., & Caprioli, D. 2021, *ApJ*, 910, 126, doi: [10.3847/1538-4357/abe2a6](https://doi.org/10.3847/1538-4357/abe2a6)
- Shu, F. H. 1992, *The physics of astrophysics. Volume II: Gas dynamics*.
- Skilling, J. 1971, *ApJ*, 170, 265, doi: [10.1086/151210](https://doi.org/10.1086/151210)
- Spitzer, Lyman, J. 1990, *ARA&A*, 28, 71, doi: [10.1146/annurev.aa.28.090190.000443](https://doi.org/10.1146/annurev.aa.28.090190.000443)
- Wentzel, D. G. 1969, *ApJ*, 156, 303, doi: [10.1086/149965](https://doi.org/10.1086/149965)
- . 1974, *ARA&A*, 12, 71, doi: [10.1146/annurev.aa.12.090174.000443](https://doi.org/10.1146/annurev.aa.12.090174.000443)
- Wiener, J., Oh, S. P., & Guo, F. 2013, *MNRAS*, 434, 2209, doi: [10.1093/mnras/stt1163](https://doi.org/10.1093/mnras/stt1163)
- Wiener, J., Pfrommer, C., & Oh, S. P. 2017, *MNRAS*, 467, 906, doi: [10.1093/mnras/stx127](https://doi.org/10.1093/mnras/stx127)
- Xu, S. 2021, arXiv:2110.08275, arXiv:2110.08275. <https://arxiv.org/abs/2110.08275>
- Xu, S., & Hu, Y. 2021, *ApJ*, 910, 88, doi: [10.3847/1538-4357/abe403](https://doi.org/10.3847/1538-4357/abe403)
- Xu, S., & Lazarian, A. 2017a, *New Journal of Physics*, 19, 065005, doi: [10.1088/1367-2630/aa6ec9](https://doi.org/10.1088/1367-2630/aa6ec9)
- . 2017b, *ApJ*, 850, 126, doi: [10.3847/1538-4357/aa956b](https://doi.org/10.3847/1538-4357/aa956b)
- . 2018, *ApJ*, 868, 36, doi: [10.3847/1538-4357/aae840](https://doi.org/10.3847/1538-4357/aae840)
- . 2020, *ApJ*, 894, 63, doi: [10.3847/1538-4357/ab8465](https://doi.org/10.3847/1538-4357/ab8465)
- . 2021, arXiv:2111.04759, arXiv:2111.04759. <https://arxiv.org/abs/2111.04759>
- Xu, S., Lazarian, A., & Yan, H. 2015, *ApJ*, 810, 44, doi: [10.1088/0004-637X/810/1/44](https://doi.org/10.1088/0004-637X/810/1/44)
- Xu, S., Yan, H., & Lazarian, A. 2016, *ApJ*, 826, 166, doi: [10.3847/0004-637X/826/2/166](https://doi.org/10.3847/0004-637X/826/2/166)
- Yan, H., & Lazarian, A. 2002, *Physical Review Letters*, 89, B1102+, doi: [10.1103/PhysRevLett.89.281102](https://doi.org/10.1103/PhysRevLett.89.281102)